Journal of The Physical Society of Japan
Vol. 60, No. 5, May, 1991, pp. 1799–1813

Anisotropic Optical Spectra of $YAlO_3$ (YAP) Single Crystals in the Vacuum Ultraviolet Region

Tetsuhiko TOMIKI, Minoru KAMINAO,* Yoshikazu TANAHARA,**
Tomoyoshi FUTEMMA,** Masami FUJISAWA† and Fujito FUKUDOME***

Department of Physics, Faculty of Science, University of the Ryukyus, Nishihara, Okinawa 903-01
†*Synchrotron Radiation Laboratory, The Institute for Solid State Physics, University of Tokyo, Tanashi, Tokyo 188*

(Received December 13, 1990)

Optical spectra of $YAlO_3$ (YAP) single crystals are measured for $\langle a \rangle$, $\langle b \rangle$ and $\langle c \rangle // E$ in the region from 6.5 eV to 42 eV by use of a plane polarized synchrotron radiation, E being the electric field of light. Anisotropic spectral behaviour of the intrinsic absorption including the tail absorption is found, and a tentative interpretation of spectral features is given in terms of the energy levels of the constituent atoms of YAP. It is found that the principal factor determining the interband absorption onset position is the bond length of Y^{3+}–O^{2-} in the compounds of Y_2O_3, YAP and YAG. The steepness constants σ_{s0} of these compounds are found to decrease in magnitude with increasing deviation from the mean value of the Y^{3+}–O^{2-} bond lengths participated in the tail absorptions.

§1. Introduction

It is already about 20 years since the advent of high quality single crystals of $YAlO_3$ (YAP) employing the Czochralski technique.[1] Greater part of spectroscopic studies have been directed to investigations from view point of development of YAP laser which may be preferable to YAG laser. These studies have accumulated a great deal of informations on the spectra displayed in the transparent region of YAP either by $4f^n$ electrons of rare earth ions doped[2,3] or by colour centres induced with the irradiation of light from a Hg-arc,[4] etc. On the contrary, only single paper dealing with the electronic spectra of YAP in the VUV[5] came to our attention. These spectra were derived, however, from the reflectivity spectrum which was measured on the natural surface of $YAlO_3$ boule grown by the Czochralski technique with the use of natural light, in spite of the fact that YAP single crystals are classified into the optical biaxial group. The information provided by ref. 5 was not sufficient for our own research on the synthesis of fast decay phosphor YAP:Ce^{3+},[6] and this stimulated the present experimental work to be carried out.

In this paper we report on anisotropic spectra of YAP single crystals measured by a plane polarized light from $\sim$6.5 eV to $\sim$42 eV and interpret their features in terms of the energy levels of the constituent atoms. Preliminary account of the results were reported previously in brief notes.[7–9] More extensive descriptions are given here on the tail absorptions and several optical functions (refractive indices, dielectric constants, loss functions, etc.). It is found that the position of the interband absorption onset depends closely on the bond length of Y^{3+}–O^{2-} in a series of compounds of Y_2O_3, $YAlO_3$ and $Y_3Al_5O_{12}$ (YAG). The steepness constants σ_{s0} of the intrinsic tails of these compounds are found to decrease in magnitude with the increase of the deviation from the mean value of the interionic distances of Y^{3+}–O^{2-} bonds participated in the tail absorptions.

* Present address: Taiyo Co., Ltd., 1-8-30 Fujiidera, Osaka 583.
** Present address: Okinawa Prefectural Government, Naha 900.
*** Present address: Fujitsu Co., Ltd., 1015 Kamikodanaka, Nakahara, Kawasaki 211.

§2. Experimental Procedures

Single crystals of YAP were purchased from the Nippon Electric Corp. (NEC). The working planes of specimens were prepared by a mechanical polish and subsequent chemical etch in hot H_3PO_4 to remove the polished surface layers. The crystallographic directions of specimens, $\langle a\rangle$, $\langle b\rangle$ and $\langle c\rangle$, were determined before cutting and confirmed after the etching by the X-ray diffraction pattern.

The anisotropic optical spectra of the absorption in the tail region and of the reflectivity were measured with the use of the plane polarized synchrotron radiation monochromatized by the Seya-Namioka type VUV monochromator (1 m grating, 1200 lines/mm) at the beam line 1 of SRL (the Synchrotron Radiation Laboratory), ISSP (Institute for Solid State Physics). The wavelength scale of the monochromator was checked and corrected by comparing the reflectivity profile in the lowest energy exciton doublet region of NaCl single crystal with that published in ref. 10 which was measured with the many-line spectrum of the hydrogen discharge light source, the wavelength of each line being calibrated and given in the literature.[11] The accuracy of the wavelength scale thus corrected was confirmed to be sufficiently good for the present experimental purposes, as recognized by inspecting the tail spectra (cf. Figs. 1 and 2).

The reflectivity spectra were measured with the spectral slit width $\Delta\lambda$ of 3 Å or 4 Å; the tail spectra were with $\Delta\lambda=4$ Å at room temperature and 2 or 3 Å at 78 K and 10 K. To minimize the effects due to the synchrotron radiation decay in intensity with time on experimental results, measurements of reflectivity (transmittance) spectra were carried out as follows: 1) The incident light intensity $I_0(\lambda)$ and the output $I_{0M}(\lambda)$ from a detector monitoring a state of the source ring are simultaneously recorded on scanning the monochromator in a spectral interval selected beforehand; 2) subsequently to 1), the reflected light intensity $I_r(\lambda)$ and the monitoring output $I_{rM}(\lambda)$ which means the monitoring output when $I_r(\lambda)$ is being measured, are taken in the same way as in 1); 3) a reflectivity in the selected region is deduced by taking the ratio

$$\frac{I_r(\lambda)/I_{rM}(\lambda)}{I_0(\lambda)/I_{0M}(\lambda)}.$$

The source of troubles may enter in this stage of the data processing because of the measurements of $I_0(\lambda)$ and $I_r(\lambda)$ at different states of light source, as detailed in ref. 12. The transmittance spectra are similarly obtained by measuring the transmittance signal $I_t(\lambda)$ instead of $I_r(\lambda)$. The monitor detector was a combination of a sheet of mesh sprayed with sodium salicylate powder and photomultiplier tube which was placed just behind the excit slit.

§3. Results and Interpretations

3.1 Tail spectra

The absorption constant $A(E, T)$ in the tail region of YAP crystals at room temperature, $T=78$ K and 10 K is shown in Figs. 1 and 2, E being the photon energy. Here, $A(E, T)$ is determined from the transmittance T_r and reflectance R' via

$$T_r=(1-R)^2\frac{\exp(-Ad)}{1-R^2\exp(-2Ad)},$$
$$R'=R+RT_r\exp(-Ad),$$

R being the intensity reflectivity from a single surface.

The thicknesses, d, of specimens employed were $1\text{ mm}\gtrsim d\gtrsim 0.04\text{ mm}$ for $\langle a\rangle /\!/ E$ and $\langle c\rangle /\!/ E$, while they were $1\text{ mm}\gtrsim d\gtrsim 0.1\text{ mm}$ for $\langle b\rangle /\!/ E$, E being the electric field of light.

Figure 1 shows the tail spectra measured for the orientation of $\langle b\rangle /\!/ E$ at $T=291$ K, 78 K and 10 K, the filled curves of $A<10^3\text{ cm}^{-1}$. The spectral behaviour of the intrinsic tail, the steeply rising part of the spectrum, is represented by a broken line at each temperature which shifts to higher energies with decreasing temperatures and converges to a point, the open circle in the figure. The absorption lying in the lower energy side of the broken line at each temperature is due to the presence of impurities and/or imperfections and tails down into the visible region as reported previously in Fig. 1 of ref. 8. The tail spectra measured for $\langle a\rangle /\!/ E$ and $\langle c\rangle /\!/ E$ at $T=296$ K, 78 K and 10 K are similarly plotted

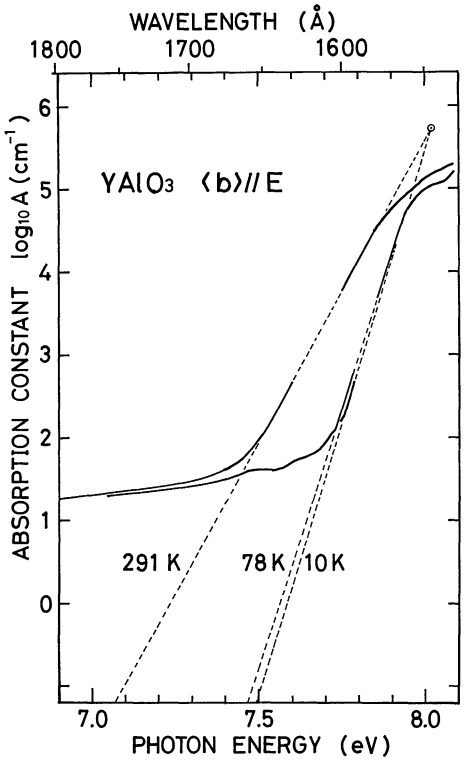

Fig. 1. The absorption spectra $A(E, T)$ in the tail region of YAP single crystals for $\langle b\rangle // E$ (the full curves $A(E, T) < 10^3\ \mathrm{cm}^{-1}$). The exponential dependence on E of the intrinsic tails is shown by the broken lines converging to a point (open circle). The full curves $A(E, T) \gtrsim 10^4\ \mathrm{cm}^{-1}$ have been transformed from the reflectivities by the Kramers-Kronig relation.

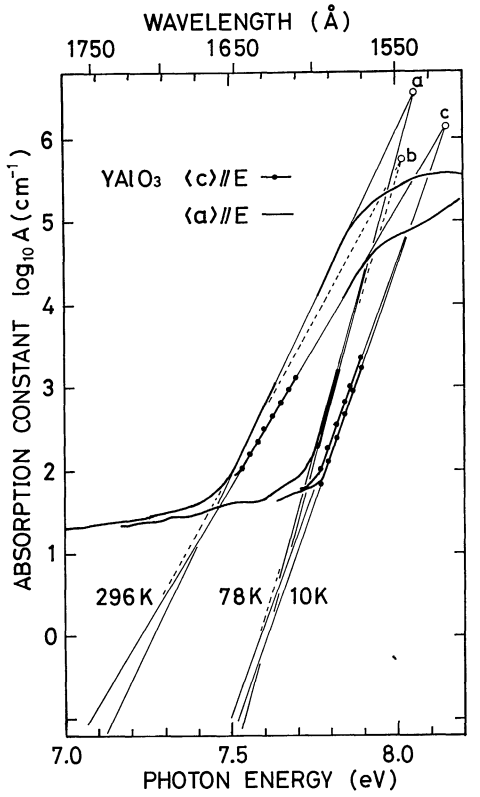

Fig. 2. The absorption spectra of YAP single crystals for $\langle a\rangle // E$ and $\langle c\rangle // E$ shown respectively by the full and dotted full curves of $A(E, T) \lesssim 1.6 \times 10^3\ \mathrm{cm}^{-1}$. The convergence point of the thinner lines representing the exponential behaviour of the intrinsic tails is denoted by a for $\langle a\rangle // E$ and c for $\langle c\rangle // E$. The exponential lines for $\langle b\rangle // E$ at 291 K and 10 K are shown by the broken lines together with the convergence point b. The full curves $A(E, T) \gtrsim 10^4\ \mathrm{cm}^{-1}$ have been derived from the reflectivities by the Kramers-Kronig relation.

with full curves of $A \lesssim 1.6 \times 10^3\ \mathrm{cm}^{-1}$ in Fig. 2. Here, the intrinsic tail, a steeply rising part of the spectrum, is also measured to shift towards the higher energy side with the decrease in temperature for each orientation as for $\langle b\rangle // E$ in Fig. 1. The convergence point of thinner lines representing the spectral behaviour of the intrinsic tails for each orientation is shown by the open circle specified with characters a and c for $\langle a\rangle // E$ and $\langle c\rangle // E$, respectively. For comparison, the spectral behaviour of the intrinsic tails for $\langle b\rangle // E$ at $T = 291$ K and 10 K is shown by broken lines together with the convergence point b. It is found that the intrinsic tails for $\langle a\rangle // E$ and $\langle b\rangle // E$ are located at nearly the same spectral position for each temperature, while for $\langle c\rangle // E$ they are in the higher energy region. A tentative interpretation on this phenomenon will be given in §3.3.2.

The tail spectra in the intrinsic region may be expressed by the well-known Urbach rule

$$A(E, T) = A_0 \exp\left(-\frac{\sigma_s(T)(E_0 - E)}{kT}\right), \quad (1)$$

$$\sigma_s(T) = \sigma_{s0} \frac{2kT}{\hbar\omega} \tanh\left(\frac{\hbar\omega}{2kT}\right). \quad (2)$$

A set of the parameters (E_0, A_0) stands for the coordinates of the convergence point of the intrinsic tails, and the steepness constant σ_{s0} and frequency $\hbar\omega$ were determined by the procedure appended in ref. 13. The result is listed in Table I. As seen in Fig. 3, the curves $\sigma_s(T)$

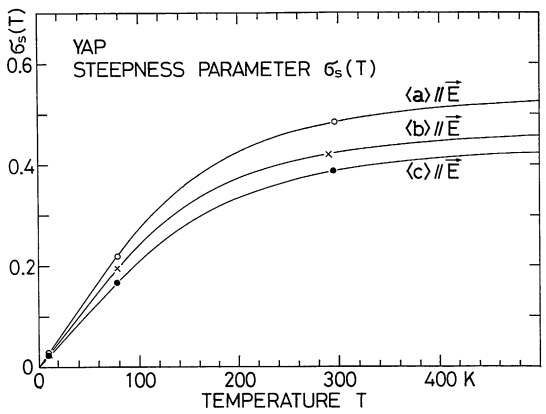

Fig. 3. The temperature dependence of the steepness parameter $\sigma_s(T)$. The full curves are calculated by eq. (2) with the use of the values of σ_{s0} and $\hbar\omega$ listed in Table I for $\langle a\rangle // E$, $\langle b\rangle // E$ and $\langle c\rangle // E$. The measured values of $\sigma_s(T)$ are shown by ○, × and ● for $\langle a\rangle // E$, $\langle b\rangle // E$ and $\langle c\rangle // E$, respectively.

Table I. The parameters E_0, A_0, σ_{s0} and $\hbar\omega$ of the Urbach rule determined by the tail spectra of YAP single crystals.

	E_0 [eV]	A_0 [cm^{-1}]	σ_{s0}	$\hbar\omega$ [meV]
$\langle a\rangle // E$	8.056	$10^{6\,53}=3.39\times10^6$	0.552	33.5
$\langle b\rangle // E$	8.018	$10^{5\,72}=5.27\times10^5$	0.479	32.5
$\langle c\rangle // E$	8.151	$10^{6\,12}=1.32\times10^6$	0.448	35.8

calculated by eq. (2) employing the values of σ_{s0} and $\hbar\omega$ in Table I well fit the steepness parameters $\sigma_s(T)$ as measured (○, × and ● for $\langle a\rangle // E$, $\langle b\rangle // E$ and $\langle c\rangle // E$, respectively). The steepness constant σ_{s0} gives a measure of the inverse of the electron-phonon coupling coefficient in the process of a photocreation of the exciton and $\hbar\omega$ is the average energy of the phonons participated.[14]

The infrared reflection spectrum, i.e., the TO phonon spectrum, of YAP at 300 K and the vibronic spectra associated with the $^2E\rightarrow{}^4A_2$ fluorescence of Cr^{3+} and with the $^2F_{5/2}\rightarrow{}^2F_{7/2}$ fluorescence of Yb^{3+} of YAP at 77 K were reported in refs. 2 and 3. The vibronic spectra and its intensity are a measure proportional to a product of the mode density and the coupling coefficient of the various phonons. Since Yb^{3+} ions reside at Y^{3+} sites and Cr^{3+} ions at Al^{3+}, the coupling of vibrations to ions at the two sites may not be identical. Nevertheless, our phonons, 32.5 meV [262.2 cm^{-1}] $\lesssim\hbar\omega\lesssim$ 35.8 meV [288.8 cm^{-1}], can be located in the lower energy region of the above two vibronic spectra extending from $\sim$100 cm^{-1} to $\sim$700 cm^{-1}.

Hole centres dealt with in ref. 4 were created with the irradiation of a Hg-arc light which covers the energy region probably up to 6.70 eV (185 nm) at highest. Thus it is to be noted that these centres are products from photochemical processes taken place in the extrinsic region of YAP, since the onset of the intrinsic absorption is located in the region $E\gtrsim$7.0 eV (see, Figs. 1 and 2).

3.2 *Spectra of reflectivity and optical constants*

The anisotropic reflectivity spectra of YAP single crystals at room temperature are shown by full curves for $\langle a\rangle // E$, $\langle b\rangle // E$ and $\langle c\rangle // E$ in Fig. 4, where the broken curves stand for the reflectivities calculated from the published data of refractive indices[15] and the dotted curve represents the reflectivity spectrum at 10 K, dotts being data points. One notices three main features there: The 1st lies in the region of 7 eV$\lesssim E\lesssim$14 eV, and the 2nd and 3rd are in the regions of 14 eV$\lesssim E\lesssim$25 eV and $E\gtrsim$25 eV, respectively. We will hereinafter refer to these as features I, II and III, respectively.

The reflectivity spectra were transformed by the Kramers-Kronig relation to the spectra of optical constants. They are the refractive index $\hat{n}=n+ik$, conductivity $\sigma=nkE$ [in eV], dielectric constant $\varepsilon=\varepsilon_1+i\varepsilon_2$, energy loss $-\mathrm{Im}\,\varepsilon^{-1}$ and the effective number of electrons per unit cell N_{eff} which is defined by the relation

$$N_{\mathrm{eff}}(E)=\int_0^E f(E)\,dE; \qquad (3)$$

$$f(E)=\frac{4mV_0}{e^2h^2}\sigma(E),$$

m and V_0 being the electron mass and the unit cell volume, respectively. In achieving the Kramers-Kronig transformation, the reflectivity function $R(E)$ adopted in the region $E\geq E_N$ was

$$R(E)=R(E_N)(E/E_N)^{-p}, \qquad (4)$$

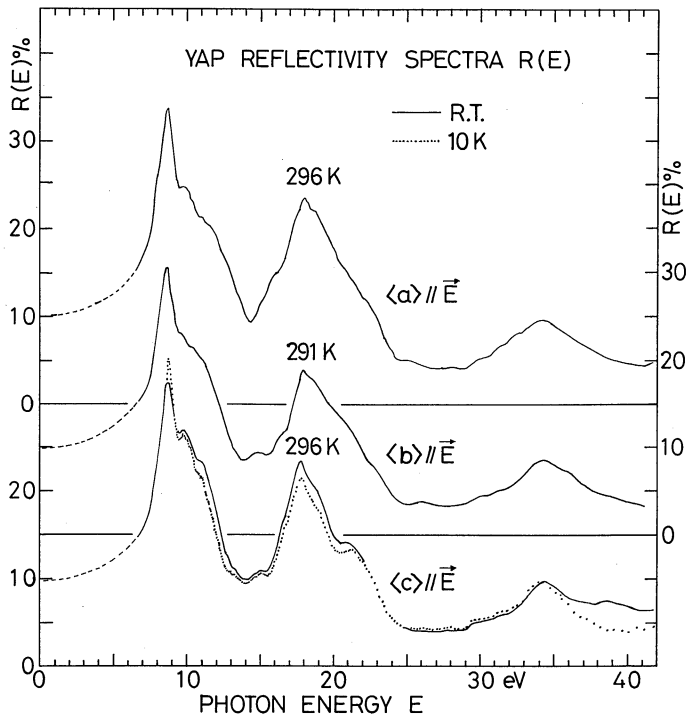

Fig. 4. The reflectivity spectra $R(E)$ of YAP single crystals for $\langle a\rangle // E$, $\langle b\rangle // E$ and $\langle c\rangle // E$. Dotts stand for the data points.

E_N being the highest energy of our experiment. The phase angle θ was selected in a way that the absorption constant $A(E)$ converted from the reflectivity conforms reasonably well to the trend of $A(E)$ measured in the intrinsic tail region. This is illustrated in Figs. 1 and 2 by the full curves of $A(E) \gtrsim 10^4\ \mathrm{cm}^{-1}$ fitting the broken or thinner lines. The resulting spectra of $\hat{n}=n+ik$ and σ are shown in Figs. 5~7 and ε, $-\mathrm{Im}\,\varepsilon^{-1}$ and N_{eff} in Figs. 8~10.

3.3 Interpretation of the spectra

3.3.1 Features II and III

The features III is most likely identified with the inner core transitions of Y^{3+} ions from the $4p^6$ to $4p^5(5s+4d)$ levels which are observed in the region from 26.20 eV to 34.84 eV on Y^{3+} free ions.[16] This interpretation is supported by the fact that a similar feature can be observed in the spectra of Y_2O_3 and $Y_3Al_5O_{12}$ (YAG) in the same spectral region.[7,8,9,17,19]

The $R(E)$ spectrum of Y_2O_3 single crystals can also be divided into three parts each of which is located in the energy region nearly the same as YAP.[17] The feature III is mentioned just above. A prominent feature is observed in the region I, while only a plateau of low intensity of ~8% can be seen in the region II. The feature I of Y_2O_3 was interpreted, in a conventional way, as arising from the transitions from the $O^{2-}2p^6$ valence bands to Y^{2+} conduction bands consisting of $4p^6(4d+5s)$ levels. The $4p^6(5d+6s)$ levels of Y^{2+} ion lie at ~10.8 eV above the ground $4p^64d$ states. Consequently, the transitions from the $2p^6$ valence to $4p^6(md+ns)$ conduction bands with $m \gtrsim 5$ and $n \gtrsim 6$ were assigned to the feature II, because they are expected to yield absorptions in the region $E \gtrsim 17$ eV where the region II is placed.

Since a prominent feature II manifests itself first in the spectra of YAP and YAG which are pseudobinary compounds of Y_2O_3 and Al_2O_3, it is believed that the feature II in these compounds is due to the absorption arising from the transitions from the $O^{2-}2p^6$ valence to Al^{2+} $3s$, $3d, \cdots$ conduction bands which is superposed with the absorption of the plateau

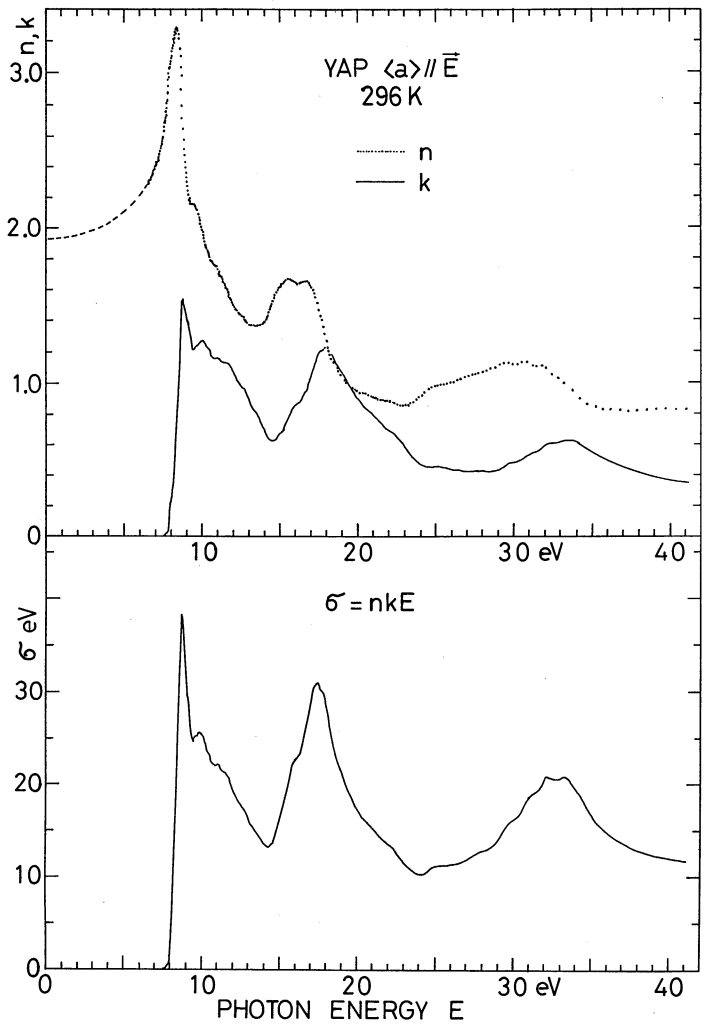

Fig. 5. The spectra of $\hat{n}=n+ik$ and $\sigma=nkE$ [in eV] of YAP single crystals for $\langle a\rangle // E$. Dotts stand for the data points.

due to Y^{2+} ions. This interpretation will not conflict with the absorption spectrum of α-Al_2O_3 single crystals whose main features are located in the region from 9 eV to 26 eV.[19]

$O^{2-}2s^2$ levels lie at $\sim$18 eV below the $O^{2-}2p^6$ levels. Hence, the transitions from the $O^{2-}2s^2$ to $Y^{2+}4p^6 5p$ bands are expected to occur in the region $E \gtrsim 26$ eV, i.e., in the region III.

3.3.2 Feature I

The feature I of YAP will be arised from the transitions from the $O^{2-}2p^6$ valence to $Y^{2+}4p^6$ $(4d+5s)$ conduction bands, at least in its lower energy part. Nevertheless, it may occur in the higher energy part of this feature that the transitions from the same valence bands to Al^{2+} $3s$, $3d, \cdots$ conduction bands participate in the photoabsorption processes. The feature I in its lower energy region to 12 eV is shown by the spectra of the reflectivity $R(E)$ and $\varepsilon_2(E)$ for $\langle a\rangle // E$ in Fig. 11. The curve $Q(E)$ stands for the excitation spectrum for Ce^{3+} emission at 360 nm of YAP:Ce^{3+} powder phosphor.[20]* A weak hump is seen

* The phosphor was prepared by a conventional ceramic technique with the addition of an appropriate flux[6] via a solid state reaction at the Matsushita Research Institute Tokyo, Inc. The phosphor was chemically etched in HNO_3 solution prior to the luminescence experiment to minimize extrinsic effects such as those due to the flux.

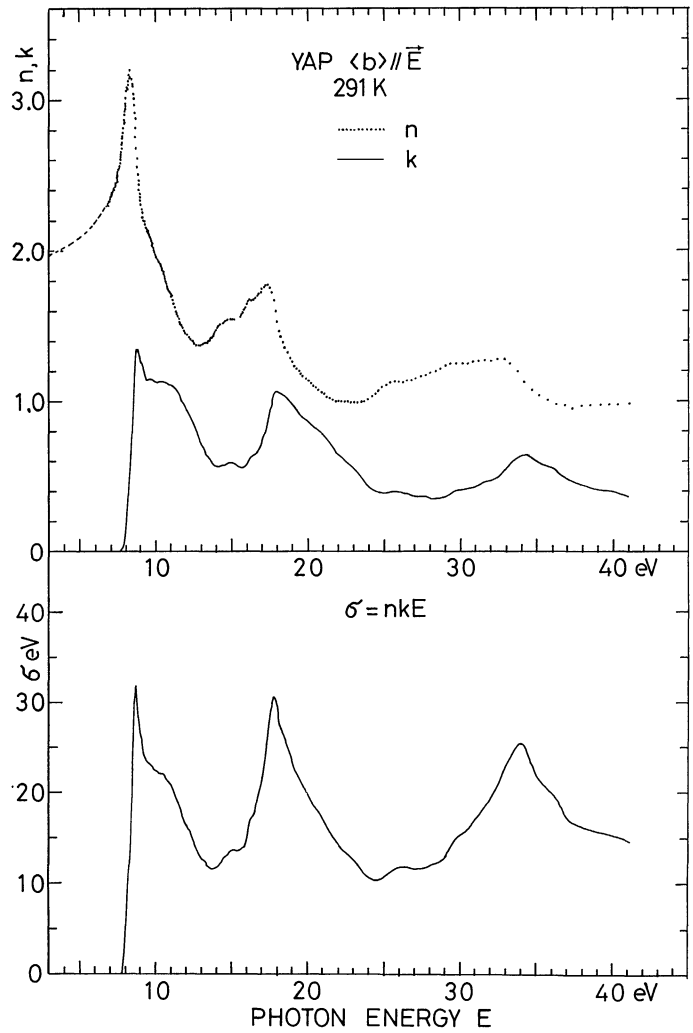

Fig. 6. The spectra of $\hat{n}=n+ik$ and $\sigma=nkE$ [in eV] of YAP single crystals for $\langle b\rangle // E$. Dotts stand for the data points.

around 8.05 eV, as indicated by an arrow, on the lower energy side of the peak of $R(E)$-spectrum at 8.70 eV. The $\varepsilon_2(E)$-spectrum similarly carries a weak hump at the same position, $E=8.05$ eV, which just corresponds to that of the convergence point of the intrinsic tails (cf. Table I). This observation is equally confirmed on the spectra of $R(E)$ and $\varepsilon_2(E)$ for $\langle b\rangle // E$. The hump is further fainter on the spectra for $\langle c\rangle // E$, but the shoulder structure can be seen around $E=8.0$ eV in the $\varepsilon_2(E)$-spectra at 296 K and 10 K as shown in Fig. 12 where the vertical lines indicate the spectral position of the convergence point c.

The excitation spectrum $Q(E)$ referring to powder phosphor shows, of course, no optical anisotropy. A steep rise of the $Q(E)$ spectrum occurs in the region $E \gtrsim 7.5$ eV towards the higher energies to $E \approx 8$ eV in parallel with the spectra of the intrinsic tails at room temperature for $\langle a\rangle$, $\langle b\rangle$ and $\langle c\rangle // E$ in Fig. 2. It will be interesting to note that the $Q(E)$ peak at 8 eV is located just in the spectral region where the convergence points (a, b and c in Fig. 2) occur and the humps of the $R(E)$ and $\varepsilon_2(E)$ spectra are observed. Similar correlation was observed on the spectra of the intrinsic tails, $\varepsilon_2(E)$ and $Q(E)$ of YAG, though the hump

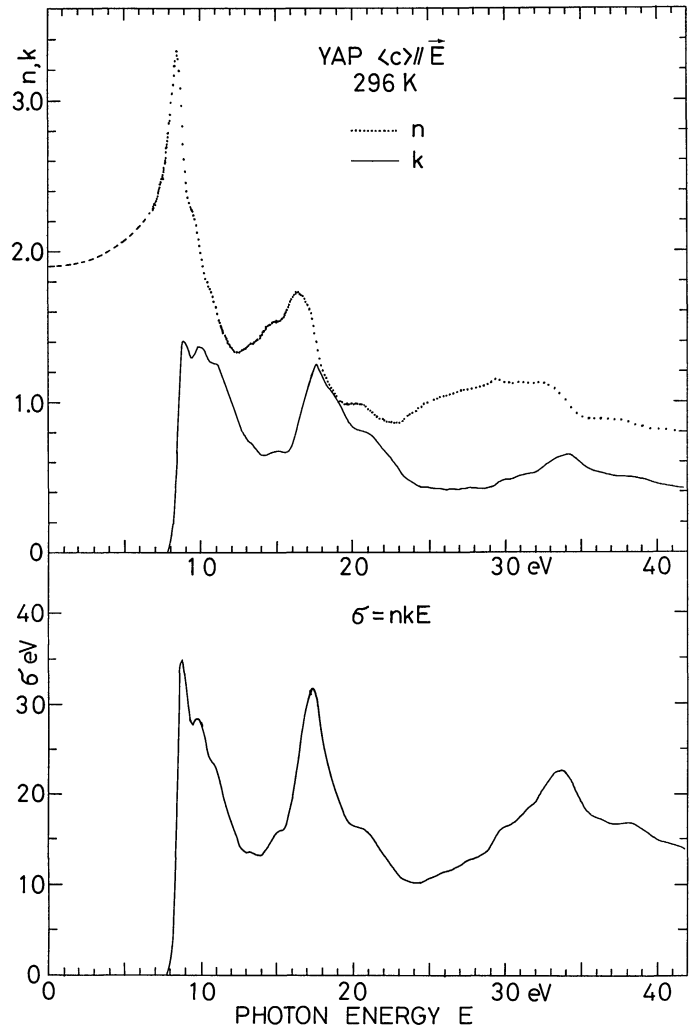

Fig. 7. The spectra of $\hat{n}=n+ik$ and $\sigma=nkE$ [in eV] of YAP single crystals for $\langle c\rangle // E$. Dotts stand for the data points.

was hardly detectable, within accuracies of the data, on the spectra of $R(E)$ at the corresponding spectral position, $E\simeq 7.0$ eV.[18] The hump of $\varepsilon_2(E)$ occurring at ~ 7.0 eV was interpreted by us as due to the excitonic absorption because of missing the photocurrent there.[21] These observations appear to indicate that the hump at ~ 8.05 eV is due to the excitonic absorption of YAP and its lower energy branch constitutes the intrinsic tails. In this case, however, there are no other data directly supporting this interpretation, to our knowledge. It is to be recalled that a description was also given in ref. 5 on the presence of this reflectivity hump together with its sharp maximum of the excitation spectra in this region for the luminescences of YAP:Eu and YAP:Nd.

If the electronic transitions from the $O^{2-}2p^6$ valence to the $Y^{2+}4p^6(4d+5s)$ conduction bands play main roles in the absorption processes in the lower energy region of the feature I, as stated above, the spectral position of the absorption onset will be expected to depend on the interionic distance between Y^{3+} and O^{2-} in lattices: To have a non-zero transition moment of the optical absorption, *e.g.*, for $\langle a\rangle // E$, at a spectral position E, the wave functions of the initial and final states for the

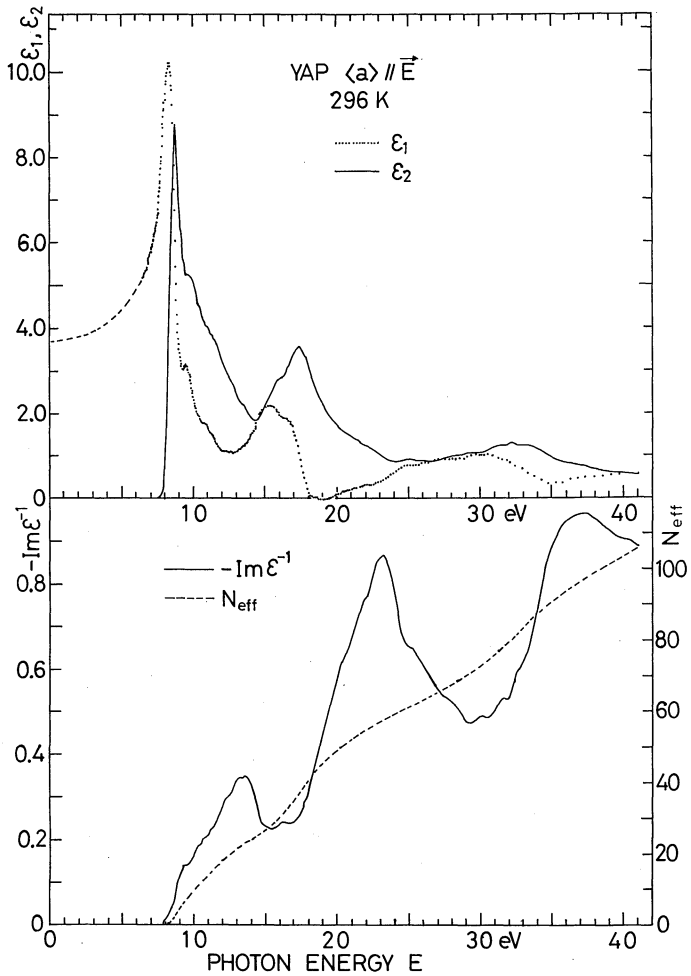

Fig. 8. The spectra of $\varepsilon=\varepsilon_1+i\varepsilon_2$, $-\mathrm{Im}\,\varepsilon^{-1}$ and N_{eff} of YAP single crystals for $\langle a\rangle // E$. Dotts stand for the data points.

transition should have their components along the bond Y^{3+}-O^{2-} lying in parallel with $\langle a\rangle$. Since these wave functions and the difference of their eigen energies, E, will be influenced with the bond length of the Y^{3+}-O^{2-}, the magnitude of the transition moment at a photon energy E must depend on the bond length of Y^{3+}-O^{2-} parallel to $\langle a\rangle$.

$YAlO_3$ crystallizes in a slightly distorted perovskite structure. Neglecting the distortion, the orthorhombic unit cell comprises four perovskitelike pseudocells. Y^{3+} ion occupies each of the eight corners of the pseudocell, O^{2-} each of six face centres and Al^{3+} the body centre. $\langle a\rangle$ and $\langle b\rangle$ of the unit cell are parallel to $\langle 110\rangle$ and $\langle 1\bar{1}0\rangle$ of the pseudocell, respectively. The Y^{3+}-O^{2-} distance of the bond chain Y^{3+}-O^{2-}-Y^{3+} parallel to $\langle a\rangle$ has two different values of 2.471 Å and 2.797 Å in the distorted orthorhombic unit cell; the mean value is 2.634 Å with $\Delta=\pm 0.163$ Å, Δ being the deviation from the mean value. These values are listed in Table II. For the bond chain Y^{3+}-O^{2-}-Y^{3+} parallel to $\langle b\rangle$, the bond length Y^{3+}-O^{2-} has also two different values as listed in Table II. We have no bond chain Y^{3+}-O^{2-}-Y^{3+} lying in parallel with $\langle c\rangle$. In this direction, there are the bond chains Al^{3+}-O^{2-}-Al^{3+} and $\cdots$-Y^{3+}-Y^{3+}-Y^{3+}-$\cdots$. It has been anticipated that the

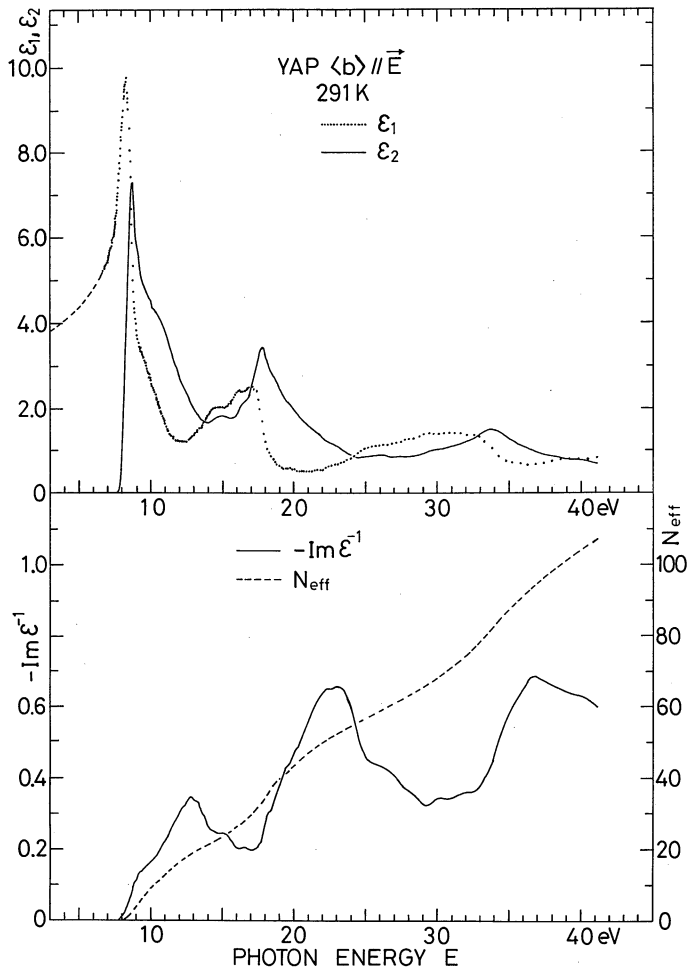

Fig. 9. The spectra of $\varepsilon=\varepsilon_1+i\varepsilon_2$, $-\mathrm{Im}\,\varepsilon^{-1}$ and N_{eff} of YAP single crystals for $\langle b\rangle /\!/ E$. Dotts stand for the data points.

former could have little contribution to the absorption in the onset region of the feature I. The optical absorptions for $\langle c\rangle /\!/ E$ in this region are to be induced by those Y^{3+}-O^{2-} bonds which are formed by Y^{3+} ion on this Y^{3+} chain and O^{2-} ion surrounding the chain with bond angles different from 90°. There are four possible pairs of Y^{3+}-O^{2-} bonds with smallest distances as listed in Table II. This contains also the bond lengths of Y^{3+}-O^{2-} in Y_2O_3 and YAG single crystals; here, each numeral in parentheses stands for the site number of Y^{3+} in the unit cell.

The convergence point of the intrinsic tails is usually located very near the spectral position of the lowest energy exciton peak in insulators.[13] Figure 1 confirms that this is valid for YAP, too: the lowest-energy lying peak of $A(E)$ at 78 K is located just at the spectral position of the convergence point. If we take the spectral position of the convergence point as a measure of the interband absorption onset position, the latter is found, in Table II, to shift to higher energy side with the increase in the bond length (average value) of Y^{3+}-O^{2-}. The exception to this is seen only in the case of the convergence point for $\langle b\rangle /\!/ E$ of YAP. On the other hand, while the bond lengths of Al^{3+}-O^{2-} are 1.91 Å for YAP and 1.97 Å and 1.86 Å (the mean value is 1.92 Å) for α-Al_2O_3,

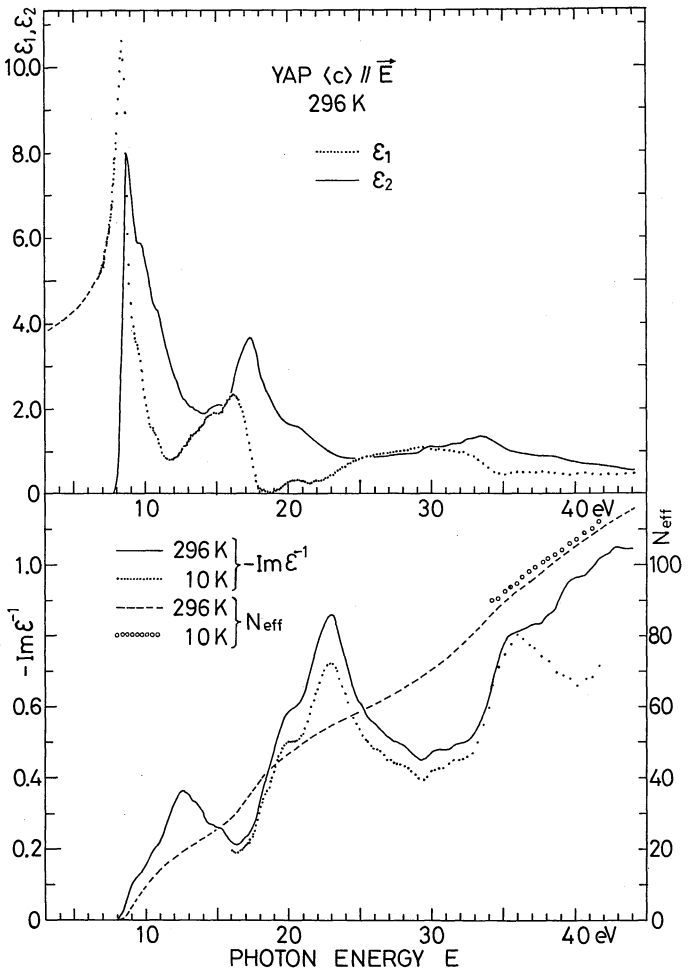

Fig. 10. The spectra of $\varepsilon=\varepsilon_1+i\varepsilon_2$, $-\mathrm{Im}\,\varepsilon^{-1}$ and N_{eff} of YAP single crystals for $\langle c\rangle // E$. Dotts and open circles stand for the data points.

the lowest energy exciton band of α-Al_2O_3 peaks at $E=9$ eV.[19] It can, thus, be said that the principal factor which determines the interband absorption onset position in a series of compounds of Y_2O_3, $Y_3Al_5O_{12}$ (YAG) and $YAlO_3$ (YAP) is the bond length of Y^{3+}-O^{2-} and is not the constituent mole number of Y_2O_3 of these pseudobinary compounds.

Alternatively, the steepness constant σ_{s0} decreases with the increase in the range of Δ in which the interionic distances of the Y^{3+}-O^{2-} bonds participated in the tail absorption vary, Δ being a deviation from the average value of the relevant bond lengths. If Δ is compared to a strain due to lattice vibrations, the above correlation found between σ_{s0} and Δ seems to be reasonable, because σ_{s0} gives a measure of the inverse the electron-phonon coupling during optical absorption.

From the viewpoint of the interionic length of Y^{3+}-O^{2-} and the deviation Δ, the spectral behaviour of the tail absorption of YAP may be stated as follows: Owing to the increase in the photon energy of the convergence point ($\approx$ the interband absorption onset) in the order of $\langle a\rangle$ and $\langle c\rangle$ and because of the decrease in magnitude of σ_{s0} in the order of $\langle a\rangle$, $\langle b\rangle$ and $\langle c\rangle$, the tails for $\langle a\rangle // E$ have been measured in the lowest energy region and the tails for $\langle c\rangle // E$ in the highest energy

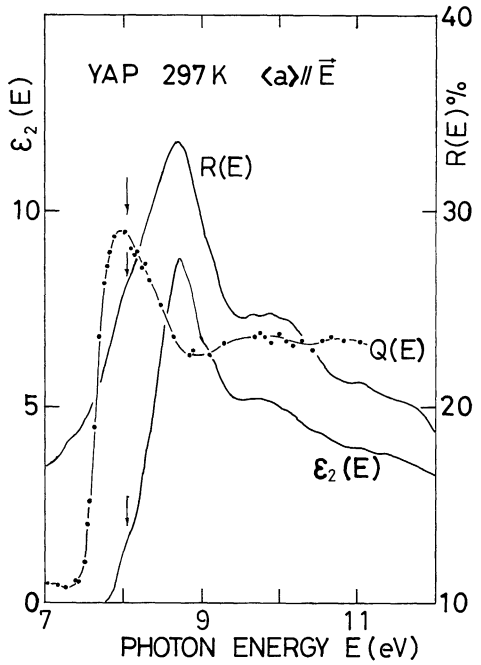

Fig. 11. The spectra of $R(E)$ and $\varepsilon_2(E)$ of YAP single crystals for $\langle a\rangle // E$ in the lower energy region of the feature I. $Q(E)$-curve represents the excitation spectrum for the Ce^{3+} emission of YAP:Ce^{3+} powder phosphor. Dotts stand for the data points.

region for $A(E) \gtrsim 10^2\ cm^{-1}$. It happens to occur that the tails for $A(E) \approx 10^0 \sim 10^1\ cm^{-1}$ are located nearly the same spectral position for $\langle a\rangle$, $\langle b\rangle$ and $\langle c\rangle // E$, (see, Fig. 2).

Figure 13 shows the anisotropic spectra $\varepsilon_2(E)$ of the feature I obtained with the plane polarized light along $\langle a\rangle$, $\langle b\rangle$ or $\langle c\rangle$. Succeeding to the main peak at 8.70 ~ 8.75 eV, weak humps around ~9.8 eV and 11 eV are seen on the spectra for $\langle a\rangle // E$ and $\langle c\rangle // E$, while the spectrum for $\langle b\rangle // E$ is on almost the monotonous decrease in intensity with the increasing photon energy. The excitation spectrum $Q(E)$ for powder phosphor YAP:Ce^{3+} carries also similar weak structures around ~9.8 eV and 10.8 eV after the passage of the dip around ~9 eV which just corresponds to the spectral position of the main peak of $R(E)$ or $\varepsilon_2(E)$. The anisotropic optical spectra $\varepsilon_2(E)$ centred on the feature II are shown in Fig. 14. Anisotropic spectral behaviour well elucidated in these figures is explicable at present in terms neither of the interband transitions nor of a primitive atomic level scheme.

3.3.3 The spectra of $N_{eff}(E)$ and $-Im\,\varepsilon^{-1}$

One notices in Figs. 8 ~ 10 the free electron like behaviour of $\varepsilon(E)$ spectra around 23 eV and 37 eV, i.e., ε_1 and ε_2 increase and decrease monotonously with the increase in E, respectively, and they are both less than unity in magnitudes. The loss peaks occur just at these two energy positions. The effective number of electrons per unit cell, N_{eff}, reaches the

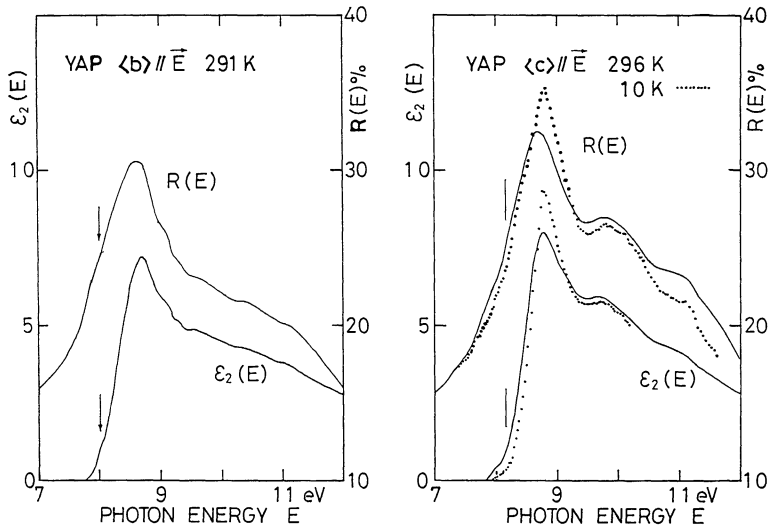

Fig. 12. The spectra of $R(E)$ and $\varepsilon_2(E)$ of YAP single crystals for $\langle b\rangle // E$ (left frame) and $\langle c\rangle // E$ (right frame) in the lower energy region of the feature I. Dotts stand for the data points.

Table II. The bond lengths of O^{2-}-Y^{3+} and tail parameters (convergence energy E_0 and steepness constant σ_{s0}) in the compounds Y_2O_3, $YAlO_3$ (YAP) and $Y_3Al_5O_{12}$ (YAG).

Compounds		Bond length O^{2-}-Y^{3+} [Å]	Average value [Å]	Deviation Δ [Å]	Convergence point E_0 [eV]	Steepness const. σ_{s0}	
Y_2O_3	$C_{3i}(8)$	2.284	2.287	−0.003	6.080	0.688	Regular octahedron
	$C_2(24)$#	2.248		−0.039			Distorted
		2.279		−0.008			Octahedron
		2.336		+0.049			
YAG	$D_2(24)$	2.293	2.369	±0.076	7.012	0.560	Dodecahedron
		2.445					
YAP*	*a*	2.471	2.634	±0.163	8.056	0.552	
		2.797					
	b	2.213	2.689	±0.476	8.018	0.479	
		3.164					
	c	2.338	2.648	−0.310	8.151	0.448	
		2.339		−0.309			
		2.656		+0.008			
		3.259		+0.611			

\# The data are calculated from ref. 22.
* The data of the bond lengths of YAP taken from ref. 23.

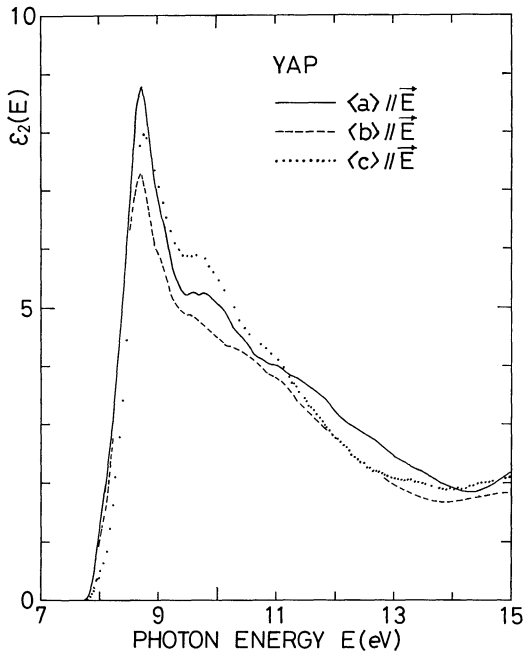

Fig. 13. The anisotropic spectral behaviour of $\varepsilon_2(E)$ spectra of YAP single crystals in the region I. Dotts stand for the data points.

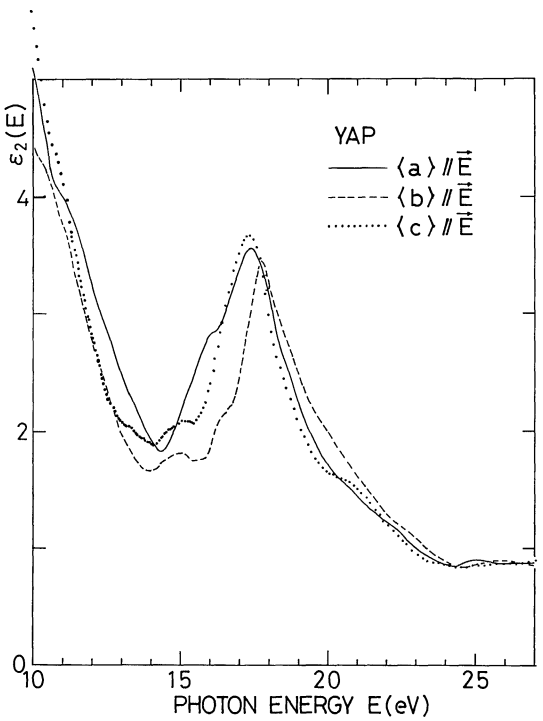

Fig. 14. The anisotropic spectral behaviour of $\varepsilon_2(E)$ spectra of YAP single crystals centred on the feature II. Dotts stand for the data points.

following values at the peak position of the loss spectra:

$N_{\mathrm{eff}}(E)=57.5$ at $E=23.22$ eV for $\langle a\rangle /\!/ E$,
52.7 23.06 eV $\langle b\rangle /\!/ E$,
55.0 23.04 eV $\langle c\rangle /\!/ E$;

and

$N_{\mathrm{eff}}(E)=97.4$ at $E=37.34$ eV for $\langle a\rangle /\!/ E$,
94.7 36.82 eV $\langle b\rangle /\!/ E$,
92.7 35.94 eV $\langle c\rangle /\!/ E$.

In view of the spectral behaviour of $\varepsilon(E)$, it is conceived that the peak at 23 eV is due to the characteristic energy loss of the collective electron oscillation in the $O^{2-}2p^6$ valence bands, and that the peak at 37 eV is caused by the collective oscillations of the electrons both in the valence bands $O^{2-}2p^6$ and in the $Y^{3+}4p^6$-bands. The unit cell of $YAlO_3$ lattice includes four formula units. Thus, the O^{2-} valence bands contain 72 electrons and $Y^{3+}4p^6$-bands 24 electrons per unit cell. It is indicated by $N_{\mathrm{eff}}(E)$-curves in Figs. 8~10 that $N_{\mathrm{eff}}=72$ at $E\sim 30$ eV and $N_{\mathrm{eff}}=72+24=96$ at ~ 37 eV. The position of the loss peak due to the plasma oscillation is, in general, sensitively affected by the presence of nearby interband transitions. Taking this into account, the above interpretation on the two loss peaks is consequently justified.

The features seen on the energy loss spectra for $E\lesssim 15$ eV is related to the one-electron transitions in this region.

The peak of $-\mathrm{Im}\,\varepsilon^{-1}$ at $E\sim 23$ eV is composed of the substructures at 20 eV, 22 eV (missing for $\langle c\rangle /\!/ E$), 23 eV and 26 eV; nevertheless, their relative intensities vary as the direction of crystallographic axes. Contrasting to this, one cannot speak of the line shape of the loss peak at 37 eV. This is because the reflectivity spectra for $E\gtrsim 35$ eV are not accurate enough for this purpose owing to the short-wave limit of the monochromator employed: Reflectivity spectra in this region show a tendency in general to increase in height towards the short-wave limit and measured with poor reproducibility. For example, owing to the enhanced background signals incorporated into the reflection signal, the apparent reflectivities at 296 K were measured larger in the region $E\gtrsim 34$ eV than those at 10 K as shown in a frame of $\langle c\rangle /\!/ E$ of Fig. 4. This affects severely the spectral behaviour of $-\mathrm{Im}\,\varepsilon^{-1}$:

While a loss peak occurs at 10 K at 36 eV, only a shoulder is suggested there at 296 K, see, Fig. 10. This type of shoulder was similarly converted around $E\simeq 36$ eV from the reflectvity spectrum of YAG at 297 K by the Kramers-Kronig relation.[18] It was directly confirmed for YAG by carrying out the electron energy loss experiment that the loss peak actually occurred at 36 eV, see, Fig. 7.[18] It is, therefore, believed that in the case of YAP the spectral behaviour of $-\mathrm{Im}\,\varepsilon^{-1}$ at 10 K is most likely and that at 296 K is false for $E\gtrsim 36$ eV. It may be interesting to note that the curve of N_{eff} at these temperatures nearly overlap with each other in the region $E\gtrsim 34$ eV and are least affected by the troubles mentioned above, as clearly seen in Fig. 10.

The absorption onset due to the transitions from $O^{2-}2s^2$-band to the conduction bands made up of the Y^{2+}- and Al^{2+}-levels was estimated as ~ 26 eV (cf. §3.3.1). The peak of the plasma oscillation including the electrons in the $O^{2-}2s^2$ band, $N_{\mathrm{eff}}=24$, is expected to occur around $E\sim 41$ eV, in view of the spectral position of the 23 eV loss peak that is apart by 15 eV from the absorption onset ~ 8 eV. To confirm this expectation, the reflectivity spectra should be measured by employing a monochromator of another type.

The present experiment had been performed at BL-1 during the period of August 1981~May 1983 under the approval of the Program Advisory Committee at the Synchrotron Radiation Laboratory, ISSP. We are grateful to Professor H. Kanzaki and Professor S. Suga and their colleagues in the SRL ISSP for supporting the present experiment. One of the authors (T. T.) is very grateful to Professor Koichi Kobayashi for allowing him to use his cryostat equipped with evacuating and detecting apparatus. He also thanks Dr. T. Miyata and Dr. T. Takeda for their giving him access to the experimental facilities in the Matsushita Research Institute Tokyo, Inc. and Dr. K. Shiroki and Dr. Y. Kuwano, Nippon Electric Corp., for their helpful information on the crystal growth and etching of

YAP. The X-ray analysis on the crystallographic axes of YAP has been carried out by Dr. Y. Kuwano, NEC. He deeply appreciates his kindness. He notes with thanks that advice by Professor M. Hosoya, University of the Ryukyus, on the crystal structure of Y_2O_3 was very helpful in calculating the Y^{3+}-O^{2-} bond lengths of a distorted octahedron.

References

1) M. J. Weber, M. Bass, K. Andringa, R. R. Monchamp and E. Comperchio: Appl. Phys. Lett. **15** (1969) 342.
2) M. J. Weber: Phys. Rev. B**8** (1973) 54.
3) M. J. Weber and T. E. Varitimos: J. Appl. Phys. **45** (1974) 810.
4) O. F. Schirmer, K. W. Blazey, W. Berlinger and R. Diehl: Phys. Rev. B**11** (1975) 4201.
5) V. N. Abramov and A. I. Kuznetsov: Sov. Phys.-Solid State **20** (1978) 399.
6) T. Takeda, T. Miyata, F. Muramatsu and T. Tomiki: J. Electrochem. Soc. **127** (1980) 438.
7) T. Tomiki, M. Kaminao, F. Fukudome and M. Seki: Activity Report on Synchrotron Radiation Laboratory ISSP (1982) p. 11; T. Tomiki, M. Kaminao, M. Seki and Y. Tanahara: *ibid.* (1983) p. 24.
8) T. Tomiki, F. Fukudome, M. Kaminao, M. Fujisawa and Y. Tanahara: J. Phys. Soc. Jpn. **55** (1986) 2090.
9) T. Tomiki, F. Fukudome, M. Kaminao, M. Fujisawa, Y. Tanahara and T. Futemma: J. Lumin. **40** & **41** (1988) 379.
10) T. Miyata and T. Tomiki: J. Phys. Soc. Jpn. **22** (1967) 209.
11) R. Onaka: *Kashi Shigai Bunkosokutei (Spectroscopic Measurements in Visible and Ultraviolet Regions)* in the *Buturi Sokutei Gijutsu (Technics of Physical Measurements)* (Asakura, Tokyo, 1967) Vol. 5, pp. 50–51, Fig. 1. 33 [in Japanese].
12) T. Tomiki, J. Tamashiro, M. Hiraoka, N. Hirata and T. Futemma: J. Phys. Soc. Jpn. **57** (1988) 4429.
13) T. Tomiki, T. Miyata and H. Tsukamoto: Z. Naturf. **29a** (1974) 145.
14) See, for example, H. Sumi and A. Sumi: J. Phys. Soc. Jpn. **56** (1987) 2211.
15) K. W. Martin and L. G. DeShazer: Appl. Optics **12** (1973) 941.
16) J. Reader, G. L. Epstein and J. O. Ekberg: J. Opt. Soc. Am. **62** (1972) 273.
17) T. Tomiki, J. Tamashiro, Y. Tanahara, A. Yamada, H. Fukutani, T. Miyahara, H. Kato, S. Shin and M. Ishigame: J. Phys. Soc. Jpn. **55** (1986) 4543.
18) T. Tomiki, F. Fukudome, M. Kaminao, M. Fujisawa, Y. Tanahara and T. Futemma: J. Phys. Soc. Jpn. **58** (1989) 1801.
19) T. Tomiki, T. Futemma, H. Kato, T. Miyahara, Y. Aiura, H. Fukutani and T. Shikenbaru: J. Phys. Soc. Jpn. **58** (1989) 1486; More reliable results are to be published in T. Tomiki, Y. Ganaha, T. Shikenbaru, S, Sato, M. Yuri, H. Fukutani, H. Kato, T. Miyahara and A. Yonesu: Photon Factory Activity Report #**8** (1990).
20) T. Tomiki, T. Miyata, T. Takeda and F. Muramatsu: unpublished work at the Matsushita Research Institute Tokyo Inc. (1977).
21) N. S. Rooze and N. A. Anisimov: Trudy Inst. Fiz. Akad. Nauk Estonian SSR. No. **44** (1975) 165.
22) Ralph W. G,. Wyckoff: *Crystal Structure* (John Wiley and Sons, New YorK, 1964) 2nd ed., Vol. 2, Chap. V, p. 1 ff, and *International Tables for Crystallography* (D. Reidel Publishing; Co., Dodrecht, Holland, 1987) p. 623.
23) R. L. Wood and W. Hayes: J. Phys. C: Solid State Phys. **15** (1982) 7209.